Toward Large Scale Roll-to-Roll Production of Fully Printed Perovskite Solar Cells

Kyeongil Hwang, Yen-Sook Jung, Youn-Jung Heo, Fiona H. Scholes, Scott E. Watkins, Jegadesan Subbiah, David J. Jones, Dong-Yu Kim, and Doojin Vak**

Solar cell technology has been developed to harvest solar energy more efficiently as well as more economically. Third-generation solar cells, including chemical-compound solar cells (CIGS, CdTe), dye-sensitized solar cells (DSSCs), and organic photovoltaics (OPVs), have been intensively studied during the past decade for their potential low production costs.[1–6] Recently, organic-inorganic hybrid perovskite solar cells have emerged as the most promising of the third-generation solar cells with an increased record of efficiency that has risen to 19.3%[7] from 3.8%[8] in last 4 years. In addition to record efficiencies published in the literature, a certified record efficiency of over 20%[9] has been reported very recently, albeit with no details disclosed. This record efficiency is already comparable to that of silicon solar cells.[9] The next challenge in the field will be translating the lab-scale process to a large-scale production process, which will preferably include a cost-competitive roll-to-roll printing process.

Organic-inorganic lead halide perovskite solar cells were initially used as the dye for DSSCs. Early perovskite solar cells were based on a mesoporous metal oxide structure that is commonly used in dye-sensitized solar cells.[8,10–12] The TiO_2 mesoporous layer in perovskite solar cells had an important role in electron transport as well as in mechanical support of the perovskite crystal as a scaffold.[12] However, mesoporous layer-based devices have a drawback in the production process as they require high-temperature sintering,[13] which precludes the use of either plastic substrates or roll-to-roll processing. To overcome the issue, the planar perovskite solar cell was developed and showed comparable performance.[14–16] The breakthrough made it possible to produce perovskite solar cells via cost-competitive roll-to-roll printing processing, and rapid progress has been made on solution-processed planar perovskite solar cells. Recently, a PCE of more than 15% has been reported for solution-processed perovskite solar cells.[17] Although rapid progress has been made, it was predominantly by the non-scalable process of spin coating. No roll-to-roll compatible process has been used to produce planar perovskite solar cells. We found only few studies that described the use of scalable solution processes. Spray coating was used to print perovskite solar cells, but only for perovskite layer.[18] Spray coating has also been explored for OPVs as a scalable coating method[19–21] since we demonstrated the first spray-coated OPV.[22] Even though the coating method is a scalable process, we found it was impractical for use in the production of solar cells due to material loss as well as the low resolution patterning of spray coating that is insufficient for a module structure. Inkjet printing was used to convert spin-coated PbI_2 layer to perovskite layer and to print carbon electrodes.[23] The process is promising as it is scalable and vacuum free. However, it will be more ideal if all layers can be printed.

The device structure of planar perovskite solar cells is similar to that of OPVs. Therefore, the processes developed for OPVs should be adaptable to the fabrication of perovskite solar cells. For the roll-to-roll fabrication of OPVs, many coating/printing methods such as slot-die coating, knife coating, spray coating, screen printing, gravure printing, flexographic printing, and inkjet printing have been studied.[24] Among the roll-to-roll compatible methods, slot-die coating has achieved the most success in the large-scale production of OPVs.[25–29] The process produces a uniform stripe with well-defined edges, which is required in conventional module design,[30] and is classified as pre-metered coating. With this process, target film thickness can be easily achieved by controlling the solution feed. In addition, this process has no loss mechanism, and all injected solutions can be transferred to the substrate.[24,25] Based on these reasons, we selected the slot-die coating method for the fabrication of perovskite solar cells.

In this report, we demonstrate the fabrication of fully slot-die coated perovskite solar cells. With the exception of evaporated metal electrode, all layers were fabricated via scalable process, slot-die coating. To develop the fabrication process, we used a 3D printer based slot-die coater that we had recently developed.[31] A typical 3D printer can control the *xyz* positions with acceleration and speed control. The temperature of the nozzle and the bed can also be controlled. Therefore, a fully PC-controlled system with temperature-control could be easily realized by adopting the existing open resources that had been developed for 3D printer.

The device configuration used in this report and its energy level diagram are shown in **Figure 1**a. The perovskite ($CH_3NH_3PbI_3$) energy levels were obtained from literature

K. Hwang, Y.-S. Jung, Y.-J. Heo, Prof. D.-Y. Kim
School of Materials Science and Engineering
Gwangju Institute of Science and Technology (GIST)
Gwangju 500–712, South Korea
E-mail: kimdy@gist.ac.kr

K. Hwang, Y.-S. Jung, Y.-J. Heo, Dr. F. H. Scholes, Dr. S. E. Watkins, Dr. D. Vak
Manufacturing Flagship, CSIRO
Clayton, Victoria 3169, Australia
E-mail: doojin.vak@csiro.au

Dr. J. Subbiah, Dr. D. J. Jones
School of Chemistry
Bio21 Institute
University of Melbourne
30 Flemington Road, Victoria 3010, Australia

DOI: 10.1002/adma.201404598

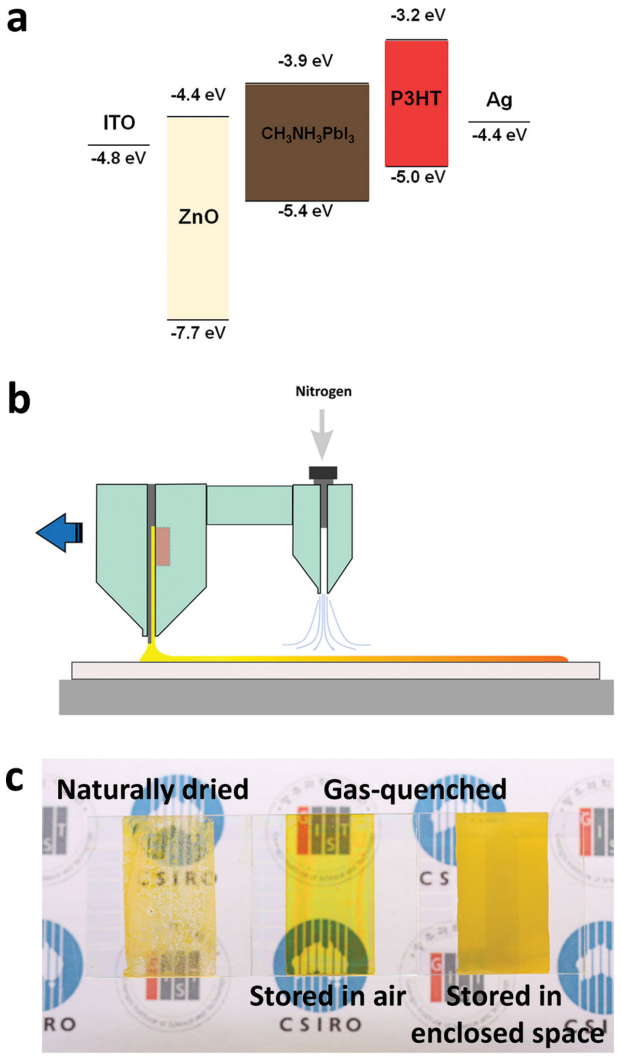

Figure 1. a) Energy-level diagram of the device used in this report. b) Schematic illustration of slot-die coating with a gas-quenching process for the fabrication of pinhole-free PbI_2 layer. c) Photographs of slot-die coated PbI_2 films under various coating conditions.

values.[8,11] Promising results with ZnO-based perovskite solar cells were reported very recently.[17] Over 15% PCE was achieved with only room temperature process. Therefore, with the exception of the coating method, we followed a process previously established in the literature. The most difficult factor in translating the spin coating process to other scalable coating/printing methods was the different drying mechanisms. In the spin coating process, the solution spreads as soon as the substrate spins and then the wet film dries while spinning at a very high speed. Therefore, there is a "quenching" step in the process. Most coating/printing methods form a wet film first, which is then allowed to dry naturally or by the use of a hot air dryer.[25] With such a slow drying step, however, the solution can flow and lose uniformity depending on the material.[24,32,33] We encountered more serious problems with the PbI_2 coating process, which consists of only small ions that rapidly form crystals. During a slow drying step, the small ions can migrate easily and form overgrown crystals, which mean that some areas on substrates are devoid of material and pinholes are formed. Naturally dried PbI_2 film is shown in Figure 1c. To stop the formation of overgrown crystals and pinholes, we introduced an external "quenching" effect to mimic the spin coating process. The first approach was to heat the substrate in order to quickly evaporate the solvent. We could obtain dense and glassy PbI_2 film by forming wet film on a heated substrate at 70 °C. However, we found the film was too dense to react with CH_3NH_3I (methylammonium iodide (MAI)) to form perovskite layer. Incomplete conversion of dense planar PbI_2 layers has already been reported by Burschka et al.[34]

Our second approach consisted of "gas-quenching." We attached an additional slot-die head to the original slot-die head for coating as shown in Figure 1b. The second head was connected to high-pressure nitrogen to quickly dry the PbI_2 film. The quenched PbI_2 film is shown in the middle of Figure 1c. The dense and uniform film could be converted to perovskite film and completed devices showed typical solar cell behavior. However, we found large batch-to-batch as well as in-batch variations with such films. We found such films could be converted to a more reactive form by using a solvent vapor soaking technique, which has been widely used for OPV.[35,36] When we stored the film in a small enclosed sample carrier as soon as coating and gas-quenching were completed, the glassy film turned cloudy, as shown in Figure 1c. The film showed a much faster conversion to perovskite when it was dipped in MAI solution, as shown in Figure S1, Supporting Information. To elucidate the phenomenon, we analyzed PbI_2 films by optical microscopy and scanning electron microscopy (SEM), as shown in **Figure 2**. It was clear that naturally dried films had insufficient surface coverage to be used in devices. The gas-quenched film showed very good uniformity. However, it was also obvious that the film was too dense to react with MAI. To fully convert to perovskite film, MAI must permeate the PbI_2 layer. The cloudy film showed the ideal form because it was dense enough to stop forming pinholes in the film, but had micro cracks that were large enough for easy permeation by MAI molecules. It is noteworthy that conversion to a cloudy form was possible only after gas-quenching. External vapor treatment did not produce such films once fully dried. We believe that the gas-quenching formed a dense, dried skin on the film, which trapped solvent inside. Therefore, the trapped solvent resulted in mobile ions that could form small crystals. Our observations on the PbI_2 films could explain the earlier difficulty in converting the planar PbI_2 layer to perovskite via a dipping process[34] when another group had reported full conversion of the layer.[17] Perovskite films and devices obtained from glassy and cloudy PbI_2 films are compared in **Figure 3**. The films were converted by dipping in MAI solution in 2-propanol following a literature procedure.[17,34] To fabricate a reference device, ZnO and P3HT hole transporting layer (HTL) were prepared by spin coating. Metal electrode was vacuum evaporated. The UV–visible absorption shown in Figure 3a clearly shows the difference in the degree of conversion for different forms of PbI_2 films. The perovskite film converted from a cloudy form shows significantly enhanced absorption-intensity over the entire spectral range between 400 nm and 800 nm.

The *J*–*V* curves of devices with slot-die coated PbI_2 layers are shown in Figure 3b. The device fabricated from the

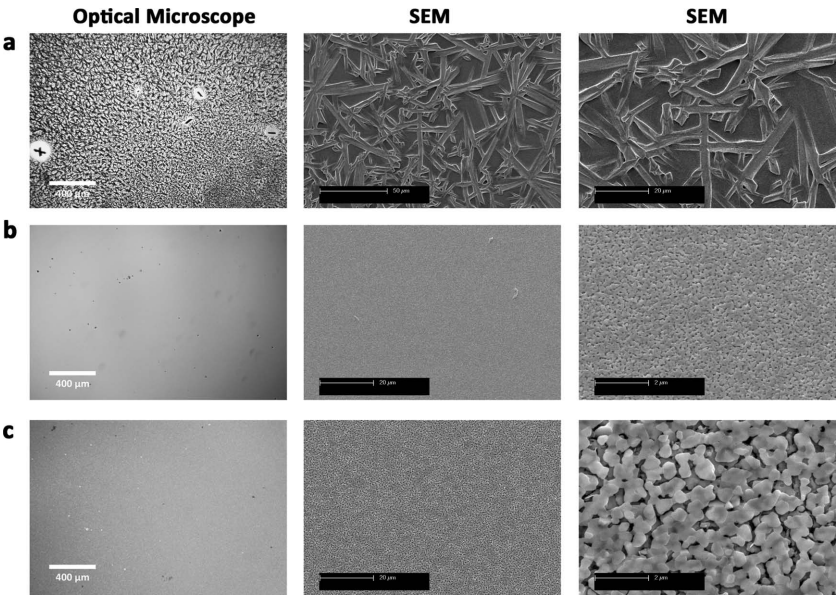

Figure 2. Optical microscopy and SEM images of the slot-die coated PbI_2 films under various coating conditions. a) The naturally dried PbI_2 film. b) The gas-quenched glassy PbI_2 film stored in air. c) The gas-quenched cloudy PbI_2 film stored in enclosed space.

glassy PbI_2 layer showed poor performance with *PCE* of 0.6% (PCE_{Avg} = 0.47%). The device fabricated from the cloudy PbI_2 layer showed a dramatically improved performance with V_{oc} = 1.00 V, J_{sc} = 19.08 mA cm^{-2}, *FF* = 62.6%, and *PCE* = 11.94% (PCE_{Avg} = 9.25%), which indicated that the device performance was strongly dependent on the PbI_2 morphology. These results were consistent with those in a previous report.[37]

Although we obtained impressive performance from the slot-die coated PbI_2 layer, all layers should be prepared by scalable methods for potential use in roll-to-roll production. Therefore, we tried slot-die coating on other layers. Because ZnO layers have been widely used for the slot-die coating for OPVs,[24] and an optimal thickness for perovskite devices has also been reported by Liu and Kelly,[17] no optimization process was carried out for the use of slot-die coated ZnO layer in the fabrication of devices. The optimal thickness, 25 nm, reported by Liu and Kelly[17] was achieved by trying various coating speeds. P3HT doped with lithium-bis(trifluoromethanesulfonyl) imide (Li-TFSI), 4-tert-butylpyridine (TBP)[38] was used for hole transporting material. There has been no previous work performed on the slot-die coating of doped P3HT on a perovskite layer; therefore, we carried out performance optimization by constructing devices under different coating conditions. The device performance was dependent on the P3HT thickness, as shown in Figure 3c. The thickness could be controlled by coating speed of the slot-die head, as we reported recently in ref.[31] The optimal thickness was found to be 142 nm obtained at 7 mm s^{-1} coating speed. Figure 3d shows the *J–V* curve characteristics of devices from spin-coated and slot-die coated ZnO and P3HT layers. We found no significant performance-reduction by introducing slot-die coated ZnO and P3HT layers. The best device showed V_{oc} = 0.98 V, J_{sc} = 20.71 mA cm^{-2}, *FF* = 57.1%, and *PCE* = 11.58% (PCE_{avg} = 9.21%), indicating that the slot-die coated ZnO and P3HT layers are as good as the spin-coated layers.

The next challenge was developing a new process for the conversion of PbI_2 to perovskite. Even though dipping is a roll-to-roll compatible process, it is not ideal to dip whole film into a solution for a minute. As an alternative to the dipping process, Chen at al. reported MAI vapor-assisted conversion process[39] and Xiao et al. reported thermally induced interdiffusion of spin-coated MAI on PbI_2 film.[40] Although the alternative approaches made excellent films followed by high device performance, those approaches require a very long annealing time, which is not adequate for large-scale production. Perovskite conversion with a short reaction time by slot-die coating would be more ideal. Therefore, to replace the MAI dipping process, we fabricated a perovskite layer via sequential slot-die coating. **Figure 4** shows SEM images of perovskite layers obtained from sequential slot-die coating. The slot-die coating of MAI at room temperature produced very small, round particles, as shown in Figure 4a, which indicated an incomplete perovskite layer. Therefore, we accelerated the conversion reaction by heating the substrates. As the temperature was increased to 50 °C, complete conversion indicated by the cubic crystals was observed. With further increases in the temperature to 70 °C, dense films with cubic-shaped crystals approximately 1 μm in size were found on the film. We found similar films from many high-performance perovskite solar cells.[17,37,41]

The degree of conversion was also confirmed by UV–visible spectroscopy, as shown in **Figure 5**a. When coating at 70 °C, the film showed comparable conversion to dipped film. We also found that the thickness of the films increased with conversion. The average thickness of a fully converted perovskite layer was approximately 500 nm. Incomplete perovskite layers were significantly thinner than fully converted ones. Thus, the UV–visible absorption intensity was well matched with the thickness variations of perovskite films that were related to the growth of perovskite crystals. To investigate the effect of processing-temperatures on device performance, we measured the *J–V* characteristics of solar cell devices with a structure of ITO/ZnO(slot die)/ perovskite(sequential slot die)/ doped P3HT(slot die)/Ag(evaporation), as shown in Figure 5b. The device parameters of fully slot-die coated perovskite solar cells are tabulated in **Table 1**. As shown in Figure 5b, the devices showed gradually improved performances with the increase of processing-temperature. The highest performance was obtained from the highest temperature, so it seemed logical to test even higher temperatures. However, we found it was difficult to print the 2-propanol solution on a substrate at higher than 70 °C, because this temperature approached the boiling point of the solvent. The room temperature coating resulted in device-performance of V_{oc} = 0.74 V, J_{sc} = 13.79 mA cm^{-2}, *FF* = 41.1%, and *PCE* = 4.20%. The best device with a slot-die coated MAI at 70 °C showed V_{oc} = 0.98 V, J_{sc} = 20.38 mA cm^{-2}, *FF* = 59.9%, and *PCE* = 11.96%. The result is comparable to the best dipping

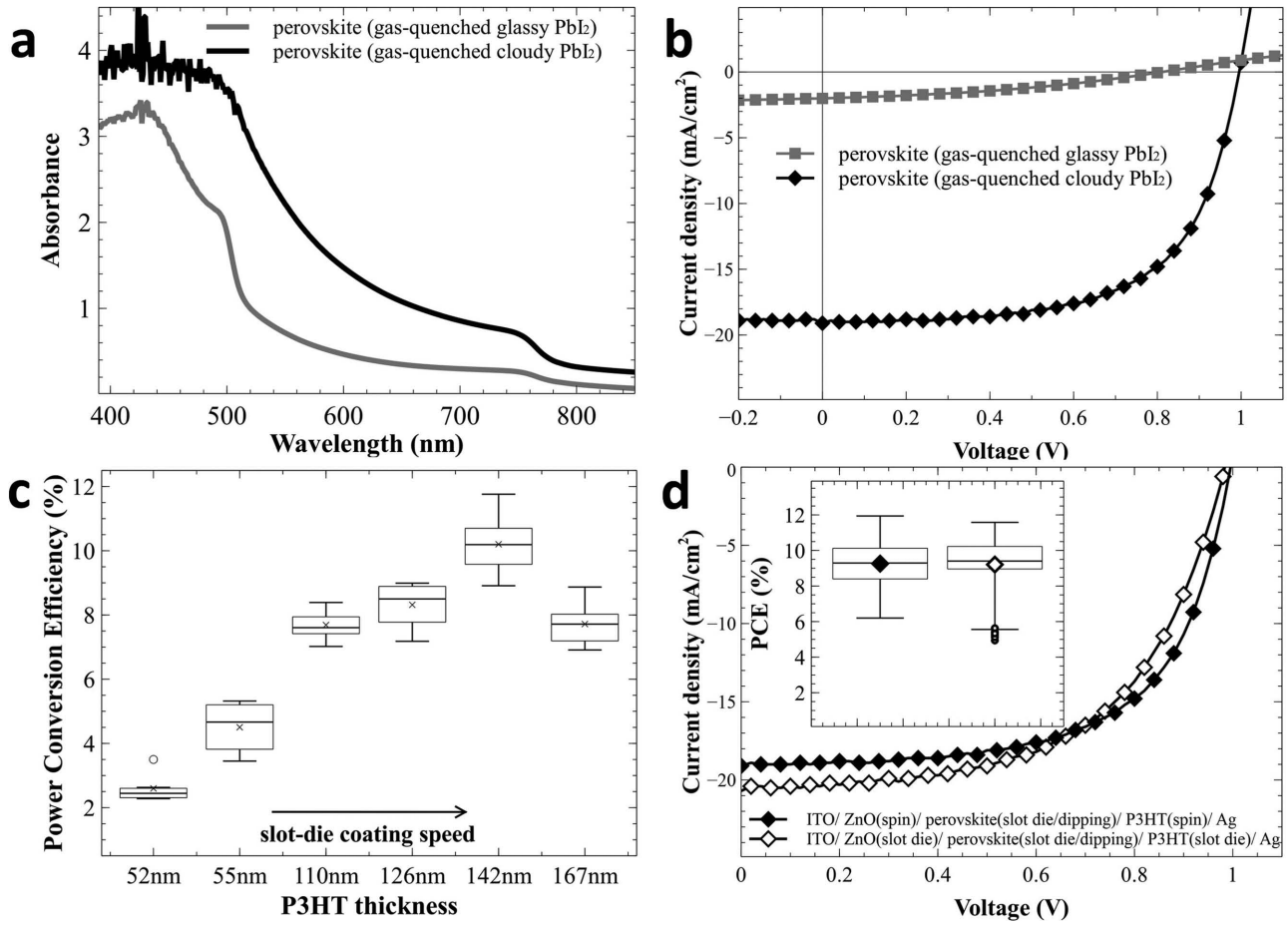

Figure 3. a) UV–visible absorption of perovskite layers processed with slot-die coated PbI_2 and MAI dipping. b) *J–V* characteristics for the highest-performing devices with structure of ITO/ZnO(spin)/ perovskite(slot die/dipping)/P3HT(spin)/Ag(evaporation). c) Power conversion efficiency distributions of 10 devices with various thicknesses of slot-die coated P3HT. d) *J–V* characteristics for the highest-performing devices and the power conversion efficiency distributions of 20 devices with the spin-coated ZnO and P3HT layers and the slot-die coated ZnO and P3HT layers.

processed perovskite solar cells. In line with previously reported issues of hysteresis in perovskite solar cells,[42–45] the efficiencies of our printed solar cells depend on the measurement conditions. The device efficiency was reduced to 9.3% in forward scan (from short circuit to open circuit). The results are shown in Figure S2 in the Supporting Information. However, we believe that the results are very promising in proving that all layers of perovskite solar cells can be printed via a roll-to-roll compatible process. To the best of our knowledge, this is the first fully printed perovskite solar cells via a roll-to-roll compatible process.

Although our results are very promising, it may be considered that the process does not seem scalable because the printed PbI_2 layer must be stored in a small chamber to be converted to the more reactive cloudy form. To confirm roll-to-roll processability of the process, we tried to improve reaction rate of MAI with less reactive glassy PbI_2 layer. Our preliminary results show that the perovskite formation reaction can be simply accelerated by increasing MAI concentration. Device performance using glassy PbI_2 was enhanced from 0.57% to 6.33% with increased MAI concentration up to 40 mg mL^{-1}. Further increases in concentration resulted in precipitation of MAI. The results are shown in Figure S3 and S4 and Table S2 and S3, Supporting Information. We believe the reaction can be further accelerated with various approaches such as different solvents with higher coating temperature. In addition, we actually translated the process to a roll-to-roll printer as shown in Figure S5, Supporting Information. The gas-quenching process could be easily adapted. A simple air blade was prepared by 3D printing and a high quality glassy PbI_2 layer could be obtained. Once glassy PbI_2 layer was prepared, the layer moved into a roll. We found the roll itself acts as a small chamber. The whole PbI_2 layer stored inside of the roll was converted to cloudy PbI_2. The layer was then easily converted to perovskite layer by slot-die coating. The results confirm the process reported in this study can be used in large scale roll-to-roll production in the future. Optimization of roll-to-roll printing process is currently under development and will be published separately.

In summary, we have demonstrated the highly efficient perovskite solar cells fully printed using slot-die coating method for the first time. Slot-die coating with gas-quenching treatment produced pinhole-free PbI_2 films. ZnO and doped P3HT charge transporting layers were also successfully fabricated via the slot-die coating method. For the fully printed perovskite device, hot slot-die coating of MAI was employed to promote

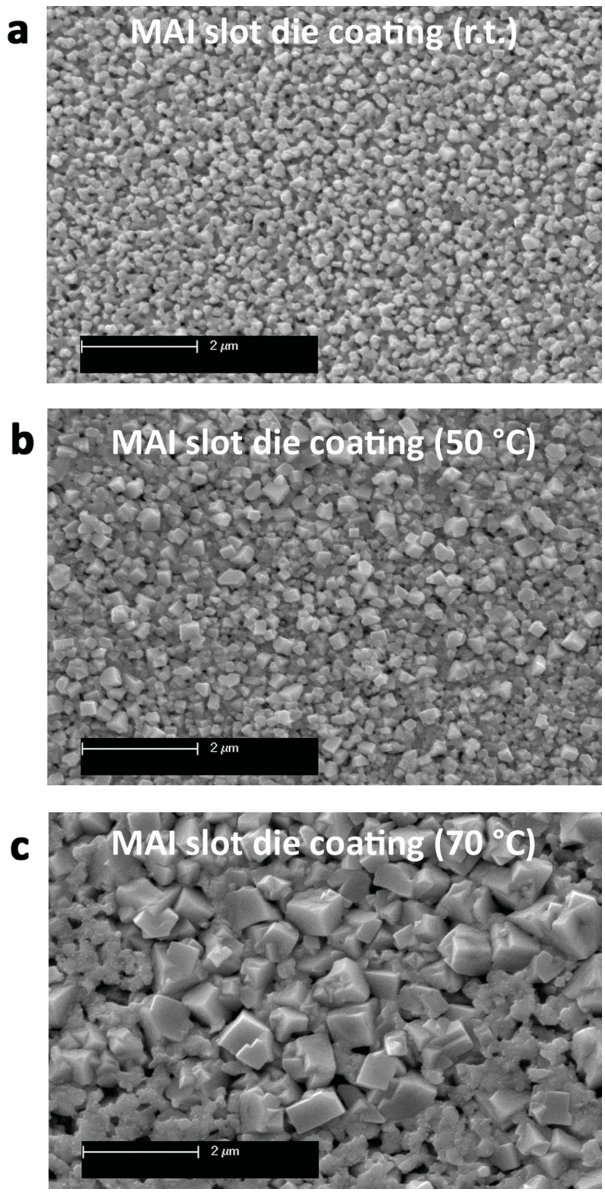

Figure 4. SEM images of the sequentially slot-die coated perovskite with various processing-temperatures. PbI_2 layers were slot-die coated and then converted to perovskite layer by slot-die coating of MAI solution at room temperature (a), 50 °C (b), and 70 °C (c).

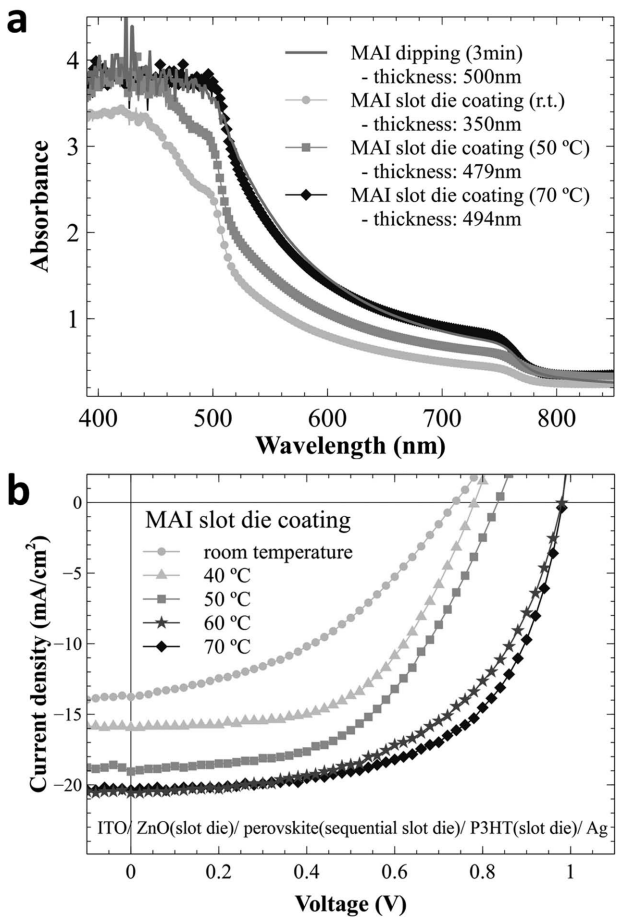

Figure 5. a) UV–visible absorption graphs of the sequentially slot-die coated perovskite layers with processing at room temperature, 50 °C, and 70 °C. b) *J–V* characteristics for the highest-performing devices with processing at room temperature, 40 °C, 50 °C, 60 °C, and 70 °C.

the conversion reaction of PbI_2 to perovskite. Well-developed perovskite crystals were observed in sequentially slot-die coated perovskite film. As a result, the best *PCE* of 11.96% was obtained from devices fabricated by slot-die coating under ambient conditions. Our results verify the possibility of the low-cost mass production of perovskite solar cells.

Experimental Section

Device Fabrication: For slot-die coated perovskite solar cell devices, ITO-coated glass (Shenzhen Display, 5 Ω sq^{-1}) was successively sonicated for 5 min each in Deconex 12PA detergent solution, distilled water, acetone, and 2-propanol. The substrates were then exposed to UV–ozone (Novascan PDS-UVT) cleaning at room temperature for 15 min. For the electron transporting layer, ZnO nanoparticles were prepared following a literature procedure.[46] The solution was coated onto ITO glass using a slot-die head with 50 μm shim and 200 μm-thick meniscus guide at 3 mm s^{-1} coating speed and 1 μL cm^{-2} solution feed. The shim with 13 mm channel was used with the same width of meniscus guide,[31] and the gap between the meniscus guide and the substrate was fixed at 100 μm. The ZnO films were then annealed at 120 °C for 10 min in air. For the perovskite layer, a PbI_2 (99%, Sigma–Aldrich) precursor solution (0.7 M, 322 mg mL^{-1}) in

Table 1. Device parameters for the fully slot-die coated perovskite solar cells under various processing-temperatures.

Processing-temperature of MAI slot-die coating [°C]	V_{oc} [V]	J_{sc} [mA cm^{-2}]	*FF* [%]	*PCE* [%]
Room temperature	0.59	13.36	45.41	3.58 (Best. 4.20)
40	0.73	15.39	46.21	5.19 (Best. 6.95)
50	0.72	17.72	53.46	6.82 (Best. 8.19)
60	0.90	19.93	50.67	9.09 (Best. 10.75)
70	0.95	19.89	53.67	10.14 (Best. 11.96)

N,*N*-dimethylformamide was prepared by stirring at 70 °C for 1 h in air. The solution was cooled to room temperature and transferred to the slot-die head without filtration. In this case, 200 μm gap between the meniscus guide and the substrate was used to maximize the wet film thickness. Coating was carried out at speed of 5 mm s^{-1} with 1 μL cm^{-2} solution feed. The wet film was then dried by N_2 gas-quenching (25 L min^{-1} through a 1 mm × 13 mm nozzle from a 25 mm distance), transferred to an enclosed sample carrier and kept in the carrier for 10 min. CH_3NH_3I was synthesized following a literature procedure[38] and 10 mg mL^{-1} solution in 2-propanol was prepared for perovskite conversion. The PbI_2 layers were dipped into the CH_3NH_3I solution for 3 min, rinsed with 2-propanol before the film dried, and then the solvent was quickly removed by N_2 gas-blowing. For the fully slot-die coated perovskite layer, the same CH_3NH_3I solution was transferred to the slot-die head without filtration and coated onto the cloudy PbI_2 layer at speed of 1 mm s^{-1} with 7 μL cm^{-2} solution feed. The PbI_2 substrates were pre-heated to various temperatures by using a heated bed in slot-die coater before CH_3NH_3I coating, and the gap between the meniscus guide and the substrate was fixed at 100 μm. When a CH_3NH_3I solution was coated onto the PbI_2 at 70 °C, the film color was changed to a dark brown immediately due to the perovskite conversion. Once perovskite layer was formed, the hole transporting layer was coated immediately to minimize exposure to moisture. For the hole transporting layer, 1 mL of P3HT (Merck) solution (15 mg mL^{-1} in chlorobenzene), 6.8 μL of Li-bis(trifluoromethanesulfonyl) imide (28.3 mg mL^{-1} in acetonitrile), and 3.4 μL of 4-tert-butylpyridine were mixed, and then transferred to the slot-die head without filtration. The solution was coated onto the perovskite film at 7 mm s^{-1} speed with 3 μL cm^{-2} solution feed without thermal treatment, and the gap between the meniscus guide and the substrate was also fixed at 100 μm. It is noteworthy that all slot-die coating processes were carried out in air. Temperature and relative humidity were typically 25–30 °C and 30–40%, respectively. For an evaporated electrode, the samples were carried to a vacuum evaporator and 100 nm of Ag was deposited through a shadow mask to produce a 10 mm^2 active area.

Measurements: The film thickness was measured using a Dektak 6M stylus surface profiler. UV–visible absorption was carried out using a Perkin–Elmer Lambda 35 spectrometer. Optical microscopy and SEM images were measured using an Olympus DP72 BH-2 (BHTU) and a Philips XL30 FEG. The *J*–*V* characteristics of the devices were measured under an inert atmosphere using Keithley 2400 Source Measure Unit with forward bias to short circuit (FB-SC) scan direction under AM1.5G, 100 mW cm^{-2} standard solar irradiation. The light intensity was calibrated using a reference cell (Hamamatsu S1133 with KG5 color-filtered window, 2.8 mm × 2.4 mm of photosensitive area), which was calibrated by a certified reference cell (PVMeasurements, certified by NREL) under 1000 W m^{-2} AM 1.5G illumination from an Oriel AAA solar simulator fitted with a 1000 W Xe lamp.

Supporting Information

Supporting Information is available from the Wiley Online Library or from the author.

Acknowledgements

This work was supported by the National Research Foundation of Korea (NRF) grant funded by the Korea government (MSIP) NRF-2010–0029212, the Flexible Electronics Group of the CSIRO Manufacturing Flagship, Victorian Organic Solar Cell Consortium [Victorian Department of Primary Industries, Victorian Department of Business and Innovation and the Australian Renewable Energy Agency (ARENA)] and the Australian Centre for Advanced Photovoltaics.

Received: October 5, 2014
Revised: November 27, 2014
Published online: January 7, 2015

[1] M. Graetzel, R. A. Janssen, D. B. Mitzi, E. H. Sargent, *Nature* **2012**, *488*, 304.
[2] T. K. Todorov, O. Gunawan, T. Gokmen, D. B. Mitzi, *Prog. Photovoltaics: Res. Appl.* **2013**, *21*, 82.
[3] B. E. Hardin, H. J. Snaith, M. D. McGehee, *Nat. Photonics* **2012**, *6*, 162.
[4] G. Li, R. Zhu, Y. Yang, *Nat. Photonics* **2012**, *6*, 153.
[5] Z. He, C. Zhong, S. Su, M. Xu, H. Wu, Y. Cao, *Nat. Photonics* **2012**, *6*, 591.
[6] C. C. Chen, W. H. Chang, K. Yoshimura, K. Ohya, J. You, J. Gao, Z. Hong, Y. Yang, *Adv. Mater.* **2014**, *26*, 5670.
[7] H. Zhou, Q. Chen, G. Li, S. Luo, T. B. Song, H. S. Duan, Z. Hong, J. You, Y. Liu, Y. Yang, *Science* **2014**, *345*, 542.
[8] A. Kojima, K. Teshima, Y. Shirai, T. Miyasaka, *J. Am. Chem. Soc.* **2009**, *131*, 6050.
[9] Research cell efficiency records, http://www.nrel.gov/ncpv, (accessed November **2014**).
[10] M. M. Lee, J. Teuscher, T. Miyasaka, T. N. Murakami, H. J. Snaith, *Science* **2012**, *338*, 643.
[11] N.-G. Park, *J. Phys. Chem. Lett.* **2013**, *4*, 2423.
[12] H. J. Snaith, *J. Phys. Chem. Lett.* **2013**, *4*, 3623.
[13] A. Yella, H. W. Lee, H. N. Tsao, C. Yi, A. K. Chandiran, M. K. Nazeeruddin, E. W. Diau, C. Y. Yeh, S. M. Zakeeruddin, M. Gratzel, *Science* **2011**, *334*, 629.
[14] M. Liu, M. B. Johnston, H. J. Snaith, *Nature* **2013**, *501*, 395.
[15] J. M. Ball, M. M. Lee, A. Hey, H. J. Snaith, *Energy Environ. Sci.* **2013**, *6*, 1739.
[16] G. E. Eperon, V. M. Burlakov, P. Docampo, A. Goriely, H. J. Snaith, *Adv. Funct. Mater.* **2014**, *24*, 151.
[17] D. Liu, T. L. Kelly, *Nat. Photonics* **2014**, *8*, 133.
[18] A. T. Barrows, A. J. Pearson, C. K. Kwak, A. D. Dunbar, A. R. Buckley, D. G. Lidzey, *Energy Environ. Sci.* **2014**, *7*, 2944.
[19] L.-M. Chen, Z. Hong, W. L. Kwan, C.-H. Lu, Y.-F. Lai, B. Lei, C.-P. Liu, Y. Yang, *ACS Nano* **2010**, *4*, 4744.
[20] C. Girotto, D. Moia, B. P. Rand, P. Heremans, *Adv. Funct. Mater.* **2011**, *21*, 64.
[21] Y.-J. Kang, D.-G. Kim, J.-K. Kim, W.-Y. Jin, J.-W. Kang, *Org. Electron.* **2014**, *15*, 2173.
[22] D. Vak, S.-S. Kim, J. Jo, S.-H. Oh, S.-I. Na, J. Kim, D.-Y. Kim, *Appl. Phys. Lett.* **2007**, *91*, 081102.
[23] Z. Wei, H. Chen, K. Yan, S. Yang, *Angew. Chem.* **2014**, *126*, 13455.
[24] R. R. Søndergaard, M. Hösel, F. C. Krebs, *J. Polym. Sci., Part B: Polym. Phys.* **2013**, *51*, 16.
[25] F. C. Krebs, *Sol. Energy Mater. Sol. Cells* **2009**, *93*, 394.
[26] T. T. Larsen-Olsen, R. R. Søndergaard, K. Norrman, M. Jørgensen, F. C. Krebs, *Energy Environ. Sci.* **2012**, *5*, 9467.
[27] D. Angmo, T. T. Larsen-Olsen, M. Jørgensen, R. R. Søndergaard, F. C. Krebs, *Adv. Energy Mater.* **2013**, *3*, 172.
[28] R. Søndergaard, M. Manceau, M. Jørgensen, F. C. Krebs, *Adv. Energy Mater.* **2012**, *2*, 415.
[29] T. R. Andersen, H. F. Dam, M. Hösel, M. Helgesen, J. E. Carlé, T. T. Larsen-Olsen, S. A. Gevorgyan, J. W. Andreasen, J. Adams, N. Li, F. Machui, G. D. Spyropoulos, T. Ameri, N. Lemaître, M. Legros, A. Scheel, D. Gaiser, K. Kreul, S. Berny, O. R. Lozman, S. Nordman, M. Välimäki, M. Vilkman, R. R. Søndergaard, M. Jørgensen, C. J. Brabec, F. C. Krebs, *Energy Environ. Sci.* **2014**, *7*, 2925.
[30] J. Yang, D. Vak, N. Clark, J. Subbiah, W. W. Wong, D. J. Jones, S. E. Watkins, G. Wilson, *Sol. Energy Mater. Sol. Cells* **2013**, *109*, 47.
[31] D. Vak, K. Hwang, A. Faulks, Y.-S. Jung, N. Clark, D.-Y. Kim, G. J. Wilson, S. E. Watkins, *Adv. Energy Mater.* **2014**, DOI: 10.1002/aenm.201401539.
[32] S. Hong, M. Yi, H. Kang, J. Kong, W. Lee, J.-R. Kim, K. Lee, *Sol. Energy Mater. Sol. Cells* **2014**, *126*, 107.

[33] M. Schrödner, S. Sensfuss, H. Schache, K. Schultheis, T. Welzel, K. Heinemann, R. Milker, J. Marten, L. Blankenburg, *Sol. Energy Mater. Sol. Cells* **2012**, *107*, 283.
[34] J. Burschka, N. Pellet, S. J. Moon, R. Humphry-Baker, P. Gao, M. K. Nazeeruddin, M. Gratzel, *Nature* **2013**, *499*, 316.
[35] M. Campoy-Quiles, T. Ferenczi, T. Agostinelli, P. G. Etchegoin, Y. Kim, T. D. Anthopoulos, P. N. Stavrinou, D. D. Bradley, J. Nelson, *Nat. Mater.* **2008**, *7*, 158.
[36] J.-S. Yeo, J.-M. Yun, D.-Y. Kim, S. Park, S.-S. Kim, M.-H. Yoon, T.-W. Kim, S.-I. Na, *ACS Appl. Mater. Interfaces* **2012**, *4*, 2551.
[37] Y. Wu, A. Islam, X. Yang, C. Qin, J. Liu, K. Zhang, W. Peng, L. Han, *Energy Environ. Sci.* **2014**, *7*, 2934.
[38] J. H. Heo, S. H. Im, J. H. Noh, T. N. Mandal, C.-S. Lim, J. A. Chang, Y. H. Lee, H.-J. Kim, A. Sarkar, M. K. Nazeeruddin, M. Graetzel, S. I. Seok, *Nat. Photonics* **2013**, *7*, 486.
[39] Q. Chen, H. Zhou, Z. Hong, S. Luo, H. S. Duan, H. H. Wang, Y. Liu, G. Li, Y. Yang, *J. Am. Chem. Soc.* **2014**, *136*, 622.
[40] Z. Xiao, C. Bi, Y. Shao, Q. Dong, Q. Wang, Y. Yuan, C. Wang, Y. Gao, J. Huang, *Energy Environ. Sci.* **2014**, *7*, 2619.
[41] P. Docampo, F. Hanusch, S. D. Stranks, M. Döblinger, J. M. Feckl, M. Ehrensperger, N. K. Minar, M. B. Johnston, H. J. Snaith, T. Bein, *Adv. Energy Mater.* **2014**, *4*, 1400355.
[42] E. L. Unger, E. T. Hoke, C. D. Bailie, W. H. Nguyen, A. R. Bowring, T. Heumuller, M. G. Christoforo, M. D. McGehee, *Energy Environ. Sci.* **2014**, *7*, 3690.
[43] H. J. Snaith, A. Abate, J. M. Ball, G. E. Eperon, T. Leijtens, N. K. Noel, S. D. Stranks, J. T.-W. Wang, K. Wojciechowski, W. Zhang, *J. Phys. Chem. Lett.* **2014**, *5*, 1511.
[44] H.-S. Kim, N.-G. Park, *J. Phys. Chem. Lett.* **2014**, *5*, 2927.
[45] N. J. Jeon, J. H. Noh, Y. C. Kim, W. S. Yang, S. Ryu, S. I. Seok, *Nat. Mater.* **2014**, *13*, 897.
[46] G. Sarasqueta, K. R. Choudhury, J. Subbiah, F. So, *Adv. Funct. Mater.* **2011**, *21*, 167.